Design and Implementation of Low-Complexity Pre-Equalizer for 1.5 GHz VLC System

Runxin Zhang, Jian Xiong, Menghan Li, and Lu Lu, *Member, IEEE*

***Abstract*—Visible light communications (VLC) has experienced rapid development in recent years as a strong competitor for next-generation wireless applications due to its wider bandwidth, higher security, and better electromagnetic immunity compared with conventional radio frequency (RF) microwaves. Although state-of-the-art VLC systems can achieve Gbps data rates by employing equalization schemes, designing a general low-complexity VLC transmitter with hundreds of MHz 3-dB bandwidth is still challenging due to the narrow modulation bandwidth nature of light emitting diodes (LEDs). In this paper, we first present a second-order equivalent circuit model for the LED, based on which we propose a general second-order equalizer (GSE) with low complexities, consisting of less than 5 passive capacitors, inductors, and resistors. We show that the GSE can enlarge the LED transmitter's bandwidth to a few hundred MHz. To validate our GSE, we build a broadband VLC transmitter using commercial-off-the-shelf (COTS) red, green and blue (RGB) LEDs, whose bandwidth is 14 MHz, by summing up three colours. Experimental results show that our proposed GSE can extend the transmitter's 3-dB bandwidth from 14 MHz to 1.5 GHz. Furthermore, we demonstrate that a VLC system utilizing the proposed GSE transmitter can achieve 1.15 Gbps data rates at a distance of 250 cm with a bit error ratios (BERs) below the forward error correction (FEC) limit 3.8×10^{-3}.**

***Index Terms*—Equalization, equivalent model, GHz bandwidth, visible light communications.**

I. Introduction

VISIBLE light communications (VLC) is an optical wireless communication technology that encodes information through variations of light intensity. By harnessing the optical spectrum, VLC promises enhanced wireless communication capabilities in terms of speed, reliability, and security when compared to traditional radio frequency (RF) and 5 G technologies [1]. Besides, a notable attribute of VLC is to simultaneously serve as an illumination source and a data transmission medium. This multifunctional capacity has garnered practical relevance in radio-sensitive settings, including industrial facilities, healthcare institutions, and aircraft [2]. The potential of VLC technology drove the development of IEEE Standard 802.15.7, initially approved in 2011 [3], defining the physical layer and medium access control sublayer for VLC. In 2019, the International Telecommunication Union (ITU) introduced the ITU-T G.9991 standard [4], derived from the ITU-T G.9961 standard. Furthermore, a task group known as Task Group bb (TGbb) was established in July 2018 to support the co-existence of Wireless Fidelity (WiFi) and Light Fidelity (LiFi) [5]. Subsequently, IEEE formally announced the IEEE 802.11bb as the Light Communication Global standard in 2023 [6].

The rapid development of VLC is closely linked to the significant progress and widespread adoption of solid-state light-emitting diode (LED) devices. In contrast to phosphor-based blue LEDs with extended recombination lifetimes due to polychromatic light, monochromatic LEDs like red, green and blue (RGB) LEDs provide a broader bandwidth. Consequently, many studies have centered on monochromatic LEDs, enabling wavelength division multiplexing (WDM) for increased data capacity. This paper also concentrates on a detailed analysis of monochromatic LEDs. Unless explicitly stated, the term *LED* in subsequent descriptions refers to monochromatic LEDs.

The limited modulation bandwidth of LEDs, typically in the range of several megahertz, imposes significant constraints on communication rates. While multi-carrier modulation schemes, including Orthogonal Frequency Division Multiplexing (OFDM), are utilized to enhance spectrum utilization, it is essential to acknowledge that the inherent modulation bandwidth of the hardware continues to be a significant limiting factor for channel capacity [7]. With the recent introduction of the IEEE 802.11bb standard [6], which extends the Medium Access Control (MAC) and Physical Layer (PHY) of IEEE 802.11 to encompass Light Communications, our aim is to design and deploy a low-complexity transmitter solution, geared towards the expansion of available bandwidth.

Equalizer is an effective device used to extend bandwidth which can be classified into pre-equalization and post-equalization, functioning at the transmitter and receiver ends, respectively. Significant contributions have been made in pre-equalization. An early work [8] in 2007 recognized the LED's low-pass characteristics and employed pre-emphasis techniques to compensate for high-frequency attenuation. In a subsequent study [9], a multiple-resonant equalization method was introduced, enabling the realization of a 4×4 LED array with a

Manuscript received 1 November 2023; revised 13 December 2023; accepted 4 January 2024. Date of publication 9 January 2024; date of current version 24 January 2024. The work of Runxin Zhang, Menghan Li, and Lu Lu was supported by the Key Research Program of the Chinese Academy of Sciences under Grant ZDRW-KT-2019-1-0103. The work of Jian Xiong was supported by the National Natural Science Foundation of China under Grant 62271044. *(Corresponding author: Lu Lu.)*

Runxin Zhang, Menghan Li, and Lu Lu are with the Key Laboratory of Space Utilization, Technology and Engineering Center for Space Utilization, Chinese Academy of Sciences, Beijing 100094, China, and also with the University of Chinese Academy of Sciences, Beijing 100049, China (e-mail: zhangrunxin20@mails.ucas.ac.cn; limenghan21@mails.ucas.ac.cn; lulu@csu.ac.cn).

Jian Xiong is with the School of Computer and Communication Engineering, University of Science and Technology Beijing, Beijing 100083, China (e-mail: b20190305@xs.ustb.edu.cn).

Digital Object Identifier 10.1109/JPHOT.2024.3351192

25 MHz bandwidth. This research also extended its scope to include a single white LED with a bandwidth of 45 MHz [10]. The bridged-T amplitude equalizer [11] accomplished equalization and impedance matching concurrently. This research group also implemented an adaptive algorithm, recursive least square for equalization [12] ultimately achieving a flat bandwidth exceeding 250 MHz for a single LED. Notably, subsequent studies in [13], [14], [15] significantly augmented bandwidth through the application of optimized T-bridge equalization techniques. Post-equalization serves as another prevalent approach for expanding bandwidth [16], [17], [18]. Furthermore, recent years have witnessed the integration of machine learning techniques [19], [20], [21] and digital equalization strategies [22], [23] within the domain of light-emitting device equalization, yielding commendable outcomes.

Among them, existing analog equalization circuits can be further classified into multiple resonant equalization circuit [9], [10], bridged-T amplitude equalizer [11], [12], [13], [14], [15], and Continuous Time Linear Equalizer [18], [26], [27]. Although these efforts have produced positive outcomes, they are predominantly rooted in empirical methodologies, which complicates their applicability to different light sources. Therefore, our work faces several challenges, including:

- The inherent uncertainty in the internal structure of light sources, which poses a significant hurdle in optical link equalization. The majority of existing efforts to broaden the 3-dB bandwidth of VLC transmitters are conducted empirically, relying on external test results, due to the unknown and complex nature of its internal structure.
- The derivation of the equalization circuit from the LED's circuit. In some previous works [14], [16], [25], the response function of the equalizer is assumed to be the reciprocal of the LED's response function. This idealized model implies that the system's frequency response can always be flattened by the equalizer, regardless of the specific input frequency, ranging from a few KHz to several GHz. Nevertheless, it is crucial to recognize that there is a substantial disparity between this theoretical model and the practical implementation of equalizers.
- Establishing a meaningful correspondence between circuit analytical expressions and real-world circuit implementations. The authors in [9], [16], [24] presented a first-order equivalent circuit for LED, only suitable for scenarios within the tens of MHz range. In [25], [28], second-order equivalent circuits were introduced, suitable for frequencies up to hundreds of MHz. Additionally, the authors of [14], [29], [30] provided higher-order circuits, including a 48th-order circuit [14] that is more suitable when the frequency is within GHz range. However, for high-order circuits, including complex second-order circuits, it is challenging to directly derive practical circuit designs from analytical expressions, not to mention developing the corresponding high-order equalization circuits.

This paper proposes a pioneering approach to address the challenges mentioned above. Unlike the traditional separation of circuit and mathematical models, this approach focuses on the LED's equivalent circuit and derives the corresponding equalization circuit using a comprehensive second-order equivalent circuit with a well-defined mathematical model. In Table I, we summarize several prior works that encompass LED circuit analysis and equalizer derivations, where B_m represents the modulation bandwidth after system equalization, and B_o is the original bandwidth without the equalizer. Additionally, the last column of Table I provides the additional parameter indicating the improvement in the achieved bandwidth, expressed as B_m/B_o. This approach proposed in this paper integrates the second-order LED equivalent circuits [28], [29], [30], and then culminating in the proposal of a second-order equalizer employing zero-pole matching methods. The main contributions are as follows:

- Diverging from experience-based transmitter equalization approaches, we have introduced a second-order equivalent circuit model for the LED. By merging this model with a second-order zero-pole matching scheme, we put forth a general second-order equalizer (GSE) that exhibits lower complexity compared to existing literature, requiring fewer than 5 passive components, including capacitors, inductors, and resistors.
- We have achieved the substantial extension of the 3-dB bandwidth of an LED transmitter to several hundred megahertz using the pre-equalizer, derived in closed-form. Following this, we have established a broadband VLC transmitter to validate our analog GSE with the commercial-off-the-shelf (COTS) RGB LEDs, which originally possess a 3-dB aggregate bandwidth of 14 MHz. Remarkably, our results demonstrate the expansion of the 3-dB bandwidth of a COTS RGB LED-based transmitter to 1.5 GHz. These findings are consistent with theoretical and implementation results in existing literature, while offering a solution with significantly lower complexity.
- We have established a VLC system utilizing the proposed GSE transmitter that achieves a data rate of 1.15 Gbps at a distance of 2.5 meters, while maintaining a Bit Error Rate (BER) below 3.8×10^{-3}.

The remainder of this paper is structured as follows: Section II delves into the analysis of the LED's equivalent circuit and the design of the GSE. Section III encompasses the presentation of the experimental setup and the corresponding test results. Lastly, in Section IV, we offer a summary of the primary findings and engage in a discussion of future research directions.

II. System Model and Circuit Design

In this section, we will commence with the establishment of an equivalent model, providing the mathematical expression for the LED's equivalent model. We will then derive the corresponding second-order GSE circuit and its response function using second-order zero-pole matching techniques.

A. Equivalent Circuit of LED

The equivalent circuit model is built mainly according to two aspects: the transport-related time constants (i.e., RC effects) of the device and the differential carrier lifetime. The inductance

TABLE I
CONTRIBUTION COMPARISON FOCUSING ON THOSE WITH DERIVATION OF EQUALIZER MODEL

Papers	Light device	LED Model	Derivation of Equalizer Model	Methods	Original 3dB Bandwidth B_o	Modulation 3dB Bandwidth B_m	Gain B_m/B_o
[9]	white×16	first-order	resonant frequency matching	multiple-resonant equalizer	2.5 MHz	25 MHz	10.00
[16]	white	first-order	reciprocal relationship	first-order equalizer	3 MHz	50 MHz	16.67
[14]	white	48th-order	reciprocal relationship	four-cascaded bridged-T network; active frequency-selecting network	30 MHz	600 MHz	20
[24]	red	first-order	zero-pole matching	RC equaliser	7.5 MHz	45 MHz	6.00
[25]	white	second-order	reciprocal relationship	digital pro-equalizer	1.5 MHz	100 MHz	66.67
This work	**RGB**	**second-order**	**zero-pole matching**	**general second-order equalizer (GSE)**	**14 MHz**	**1.5 GHz**	**107.14**

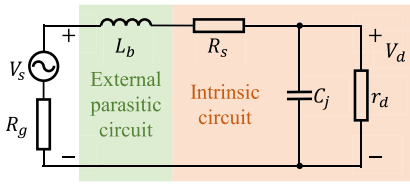

Fig. 1. Second-order equivalent model of LED is a good choice in the frequency from the DC to hundreds of megahertz.

and capacitance effects caused by different packaging structure should be considered on a case-by-case basis. Based on [29], we present a simplified second-order equivalent circuit suitable for direct current (DC) to several hundred megahertz, as depicted in Fig. 1. The figure illustrates the equivalent circuit of a turned-on LED containing two parts: an intrinsic circuit and an external parasitic circuit. The intrinsic circuit comprises the series resistance R_s, junction capacitance C_j, and the differential resistance r_d within the LED. Specifically, C_j encompasses both the diffusion capacitance C_d and the space-charge capacitance C_{sc}, collectively affecting the effective carrier lifetime τ_{eff} in conjunction with r_d as $\tau_{\text{eff}} = r_d(C_d + C_{sc}) = r_d C_j$. In the external parasitic circuit, we solely consider the series bonding inductance L_b. It's worth noting that R_g represents the output impedance of the signal source, typically set at 50 Ω. The current passing through the LED, regulated by the differential resistance r_d [31], regulates the optical output power. This relationship exists because optical power is linearly associated with the voltage of the input signal. Then, we can represent the frequency response between the voltage V_d across r_d and the alternating current (AC) signal V_s applied to the biased LED as

$$
\begin{aligned}
H_{\text{LED}}(s) = \frac{V_d}{V_s} &= \frac{\frac{1}{sC_j} \,//\, r_d}{\frac{1}{sC_j} \,//\, r_d + sL_b + R_s + R_g} \\
&= \frac{r_d}{s^2 r_d C_j L_b + s\left[L_b + r_d\left(R_s + R_g\right)C_j\right] + R_s + R_g + r_d} \\
&\overset{(a)}{\approx} \frac{\frac{r_d}{R_s + R_g}}{\left[s/\left(\frac{1}{C_j r_d}\right) + 1\right]\left[s/\left(\frac{R_s + R_g}{L_b}\right) + 1\right]} \\
&\triangleq \frac{K_{\text{LED}}}{\left[\frac{s}{\omega_{\text{LED1}}} + 1\right]\left[\frac{s}{\omega_{\text{LED2}}} + 1\right]},
\end{aligned}
\tag{1}
$$

where ω_{LED1} and ω_{LED2} are two corner frequencies of the LED, K_{LED} is the gain, and (a) follows from $r_d \ll R_s + R_g$ indicating

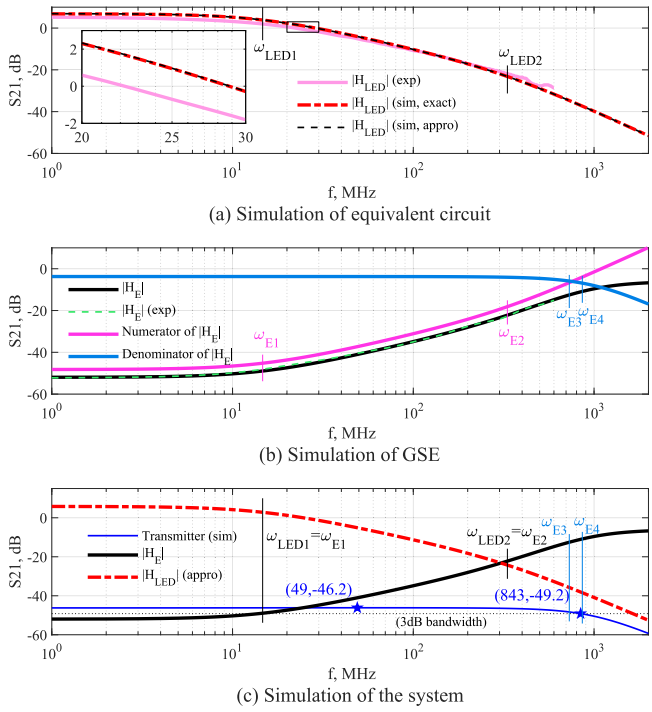

(a) Simulation of equivalent circuit

(b) Simulation of GSE

(c) Simulation of the system

Fig. 2. Comparison of the equivalent circuit, GSE circuit, and the corresponding response curves for the proposed transmitter based on this GSE.

that the second-order equivalent circuit (1) can be deconstructed into two cascaded first-order circuits.

Fig. 2(a)–(c) illustrate the response curves for the equivalent circuit, GSE circuit, and the corresponding designed transmitter based on this proposed GSE, along with an overview of the GSE design concept. Details about (b) and (c) will be elaborated in Section II-B.

Fig. 2(a) presents a comparison of three S21 response curves: one for a lit LED (Osram, LE RTB N7WM) and the other two based on (1), depicting both the exact and approximate curves. It also marks the two corner frequencie mentioned in (1). Further details about the system's test setup are presented in Section III-A. As depicted in Fig. 2(a), it is evident that these three curves display substantial overlap. The maximum estimation offset between the simulation result of $H_{\text{LED}}(s)$ and the measured result is 2.29 dB within the 500 MHz range, and it extends to a maximum offset of 3.12 dB within the 530 MHz range. However, beyond 530 MHz, the response demonstrates a complex behavior that cannot be sufficiently described by

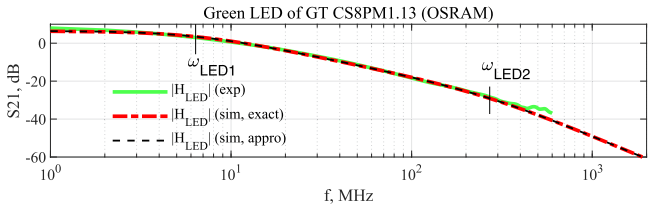

Fig. 3. Application of the proposed second-order equivalent circuit on Green LED (GT CS8PM1.13, OSRAM).

TABLE II
PARAMETER VALUES OF THE EQUIVALENT CIRCUIT AND EQUALIZER

Parameters	Value		
Equivalent Circuit	BLUE	$L_b = 28.6$nH	$R_s = 1\Omega$
		$C_j = 10.8$nF	$r_d = 0.5\Omega$
	GREEN	$L_b = 19.1$nH	$R_s = 1\Omega$
		$C_j = 12.5$nF	$r_d = 0.5\Omega$
	RED	$L_b = 24.5$nH	$R_s = 1\Omega$
		$C_j = 21.7$nF	$r_d = 0.5\Omega$
Equalization Circuit	BLUE	$L = 4.3$nH	$R_1 = 0.8\Omega$
		$C = 3.5$pF	$R_2 = 160\Omega$
	GREEN	$L = 4.7$nH	$R_1 = 0.75\Omega$
		$C = 2.5$pF	$R_2 = 150\Omega$
	RED	$L = 4.7$nH	$R_1 = 0.4\Omega$
		$C = 4.0$pF	$R_2 = 120\Omega$

the second-order equivalent circuit. Additionally, the inherent low-pass characteristic of the light source leads to significant attenuation at high frequencies, rendering the signal too weak for detection by the photodiode.

We also employed another LED device (GT CS8PM1.13, OSRAM) to validate the provided equivalent model. The results are depicted in Fig. 3: the maximum deviation between the simulation and measured results is 3.17 dB within the 460 MHz, with a mean deviation value of 0.53-dB. The subsequent analysis will follow a similar pattern, and thus, we will refrain from repeating it.

Building upon the second-order equivalent circuit, specifically the corner frequencies presented in (1) as demonstrated earlier, we will introduce a comprehensive second-order equalizer in Section II-B. In this section, we utilize the data from the red LED shown in Fig. 2 as an illustrative example, and this can be readily extended to the other two LEDs. A comprehensive list of all parameters employed in the simulation from Fig. 2 is provided in Table II, with details of their derivation covered in the Section II-C. Furthermore, a direct connection between the LED and the equalization circuit is not feasible; it requires an intermediate driver circuit, as discussed in the Appendix A.

B. Zero-Pole Matching Method

In the previous subsection, we provided an equivalent circuit model for the LED and derived the expression of its second-order response function. We validated the reliability of this expression by comparing it with the response curve of a commercially available LED through experimental measurements. In this subsection, we will derive the corresponding response expression of a general second-order equalizer based on the second-order low-pass equivalent circuit of the LED provided in the previous section, using the zero-pole matching method. This will provide theoretical support for the subsequent design of the specific equalization circuit.

We obtain the general expression for a second-order high-pass circuit as

$$H_{\mathrm{E}}(s) = \frac{K_{\mathrm{E}}\left(\frac{s}{\omega_{\mathrm{E1}}}+1\right)\left(\frac{s}{\omega_{\mathrm{E2}}}+1\right)}{\left(\frac{1}{\omega_{\mathrm{E0}}}\right)^2 s^2 + \frac{2\zeta_{\mathrm{E}}}{\omega_{\mathrm{E0}}}s + 1}, \tag{2}$$

where K_{E} represents the gain of the response function, which is the response value of the system at zero frequency, ω_{E1} and ω_{E2} are two zeros of the equalizer, and ζ_{E} and ω_{E0} denote the damping ratio and natural frequency, respectively. Combining (1) and (2), the response function of the link after cascading the LED and GSE can be represented as

$$\begin{aligned} H_{\mathrm{T}}(s) &= H_{\mathrm{LED}}(s)\cdot H_{\mathrm{E}}(s) \\ &= \frac{K_{\mathrm{LED}}}{\left[\frac{s}{\omega_{\mathrm{LED1}}}+1\right]\left[\frac{s}{\omega_{\mathrm{LED2}}}+1\right]} \cdot \frac{K_{\mathrm{E}}\left(\frac{s}{\omega_{\mathrm{E1}}}+1\right)\left(\frac{s}{\omega_{\mathrm{E2}}}+1\right)}{\left(\frac{1}{\omega_{\mathrm{E0}}}\right)^2 s^2 + \frac{2\zeta_{\mathrm{E}}}{\omega_{\mathrm{E0}}}s + 1} \\ &\overset{(a)}{=} \frac{K_{\mathrm{LED}}K_{\mathrm{E}}}{\left(\frac{1}{\omega_{\mathrm{E0}}}\right)^2 s^2 + \frac{2\zeta_{\mathrm{E}}}{\omega_{\mathrm{E0}}}s + 1} \overset{(b)}{=} \frac{K_{\mathrm{LED}}K_{\mathrm{E}}}{\left(\frac{s}{\omega_{\mathrm{E3}}}+1\right)\left(\frac{s}{\omega_{\mathrm{E4}}}+1\right)}, \end{aligned} \tag{3}$$

where (a) follows from zero-pole matching methods as we establish a correspondence between the zeros of the equalizer and the poles of the LED response, specifically, $\omega_{\mathrm{E1}} = \omega_{\mathrm{LED1}}$ and $\omega_{\mathrm{E2}} = \omega_{\mathrm{LED2}}$; (b) follows as we express them in a cascaded format without loss of generality, where ω_{E3} and ω_{E4} represent the two poles of the equalizer's response function, and we assume $\omega_{\mathrm{E3}} \le \omega_{\mathrm{E0}} \le \omega_{\mathrm{E4}}$. In contrast to the utilization of first-order zero-pole matching in [24], which achieved a 45 MHz 3-dB bandwidth, our second-order zero-pole matching method allows us to attain equalization at the GHz level.

As can be seen from (2), the derived equalizer is a non-standard second-order high-pass circuit, characterized by two zeros and two poles. Given that the position of poles and zeros determines the shape of the frequency response curve, we can attain precise equalization of the LED by designing the position of the corner frequencies, as depicted in Fig. 2(b). Fig. 2(b) presents a comparison between the response curves of the equalizer's response function (2) and the test results of the equalization circuit constructed based on this expression. To facilitate analysis, we have plotted the curves corresponding to the numerator and denominator of (2) within the same frequency range and labeled the zeros and poles of this GSE.

Fig. 2(c), the principle of zero-pole matching is illustrated. It includes a comparison of the response curves of the LED, the GSE, and the response at the transmitter after equalization. The four crossover frequencies are also marked. Additionally, Fig. 2(c) shows the highest point of the response after equalization and the location of the 3-dB bandwidth. It is evident that by carefully tuning the values of ω_{E1} and ω_{E2} to achieve $\omega_{\mathrm{E1}} = \omega_{\mathrm{LED1}}$ and $\omega_{\mathrm{E2}} = \omega_{\mathrm{LED2}}$, as illustrated in Fig. 2(c), we can effectively expand the transmitter's 3-dB bandwidth. This

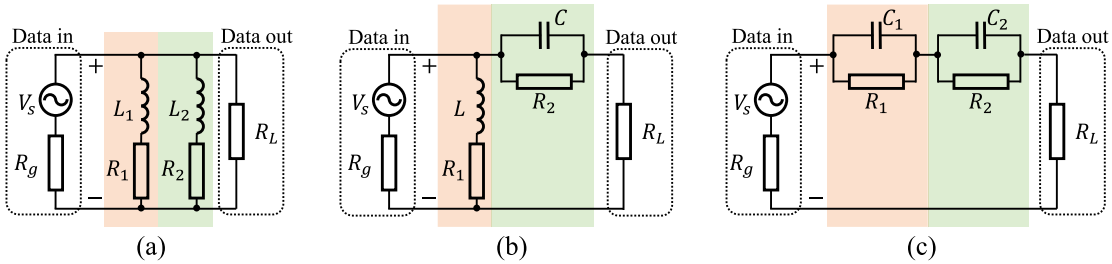

Fig. 4. Low-complexity general second-order circuit proposed in this paper. (a)–(c) are three implementation examples.

also implies that the ideal reciprocal relationship between the S21 responses of the equivalent circuit and the equalizer cannot be achieved. This section presents a low-complexity equalizer implementation based on the LED response function.

Through zero-pole matching, the poles in (2) set the upper limit on the equalization capability, as clearly illustrated in Fig. 2(c). To maximize the smaller pole ω_{E3} of the equalization circuit, we hypothesize that the maximum value of the smaller pole is attainable when $\omega_{\mathrm{E3}} = \omega_{\mathrm{E4}}$. Therefore, we can conclude that the 3-dB bandwidth of the link is determined by the smaller value between the minor pole ω_{E3} and the maximum frequency representable by the equivalent circuit – the frequency at which the deviation between the equivalent circuit and the actual test circuit remains within 3-dB. According to Fig. 2(a), the maximum frequency that the equivalent circuit can represent is approximately 550 MHz for the red LED.

C. Circuit Design of GSE

To achieve the response function described in (2), a series of low-complexity second-order models can be constructed using passive components, including capacitors, inductors, and resistors, as illustrated in Fig. 4. Without loss of generality, we will use Fig. 4(b) as an example in this section.

The inductor L and the capacitor C are used to implement the high-pass characteristic, while the resistors R_1 and R_2 play a critical role in controlling the response amplitude for frequencies near DC. The presence of these resistors is also essential in achieving the desired zeros. Consider an equalization circuit as shown in Fig. 4(b) but without resistors. In this case, the transfer function can be expressed as:

$$H(s) = \frac{s^2\, LCR_g}{2\, s^2\, LCR_g + s(CR_g^2 + L) + R_g}. \tag{4}$$

In accordance with (4), the absence of resistors in the circuit results in all zeros of this second-order circuit being positioned at the DC frequency, rendering the implementation of the zero-pole matching method unsuccessful. Therefore, the inclusion of resistors is essential to enable zero-pole matching and effectively realize the intended equalization function.

The transfer function of the equalization circuit depicted in Fig. 4(b) can be expressed as [32]

$$H_{\mathrm{E}}(s) = \frac{(sL + R_1)//\left(\frac{1}{sC}//R_2 + R_L\right)}{R_g + (sL + R_1)//\left(\frac{1}{sC}//R_2 + R_L\right)} \frac{R_L}{\frac{1}{sC}//R_2 + R_L}$$

$$\approx \frac{\frac{2R_gR_1}{(2R_1+R_g)(2R_g+R_2)}\left(\frac{s}{\omega_{\mathrm{E1}}}+1\right)\left(\frac{s}{\omega_{\mathrm{E2}}}+1\right)}{\left(\frac{s}{\omega'_{\mathrm{E3}}}+1\right)\left(\frac{s}{\omega'_{\mathrm{E4}}}+1\right)}, \tag{5}$$

where $//$ denotes a parallel configuration within the circuit; $\omega_{\mathrm{E1}} \triangleq \frac{R_1}{L}$ and $\omega_{\mathrm{E2}} \triangleq \frac{1}{CR_2}$ are defined as the zeros of the equalizer, and the approximate poles can be written as

$$\omega_{\mathrm{E3,I}} \triangleq \frac{2R_1 + R_g}{2\,L}, \quad \omega_{\mathrm{E4,I}} \triangleq \frac{2R_g + R_2}{2\,CR_gR_2}.$$

Refer to Appendix B for the detailed derivation process of (5). Employing the zero-pole matching method outlined in (2), we need to configure the zeros of the equalizer in (5) based on the poles of the LED in (1) as

$$\begin{cases} \frac{R_1}{L} = \frac{1}{C_j r_d} \\ \frac{1}{CR_2} = \frac{R_s + R_g}{L_b} \end{cases}. \tag{6}$$

Even with the knowledge of L, R_1, C, R_2, and R_g shown in Fig. 4(b), the two equations remain insufficient for determining the values of the four unknown parameters: C_j, r_d, R_s, and L_b in Fig. 1. Drawing from references [29], [30], we make reasonable assumptions that set r_d to $0.5\,\Omega$ and R_s to 1Ω. With these assumptions, we can calculate all the parameter values in the LED equivalent circuit. This entails setting the component parameters in the circuit illustrated in Fig. 4(b) to achieve equalization. The parameters used in the final configuration are presented in Table II. As shown in Fig. 2(a)–(b), the measured curve and the simulated curve largely overlap. Furthermore, as depicted in Fig. 2(c), the resulting 3-dB bandwidth is not less than the smaller pole $\omega_{\mathrm{E3,I}}$ of the equalizer, aligning with the analysis in II-B.

III. Experimental Results

In the previous section, we established the equivalent circuit for the LED and rigorously derived a general second-order equalizer response function using zero-pole matching. Based on this expression, we provided a range of low-complexity implementation options with specific parameters. This section will provide details about the experimental system setup and the performance of the transmitter equipped with the proposed GSE. The performance evaluation will primarily focus on the 3-dB bandwidth, as well as the communication speed of the optical link established by the broadband VLC transmitter.

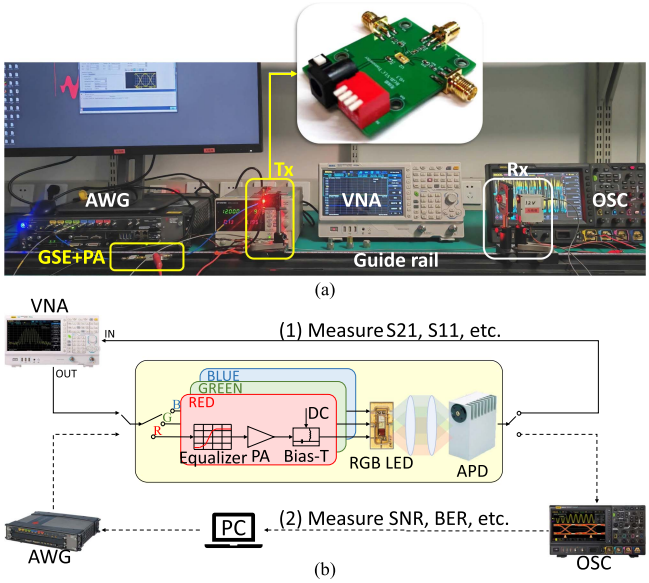

Fig. 5. System setup. (a) Depicts the experimental configuration. (b) Illustrates block diagrams of the system with two different connection methods.

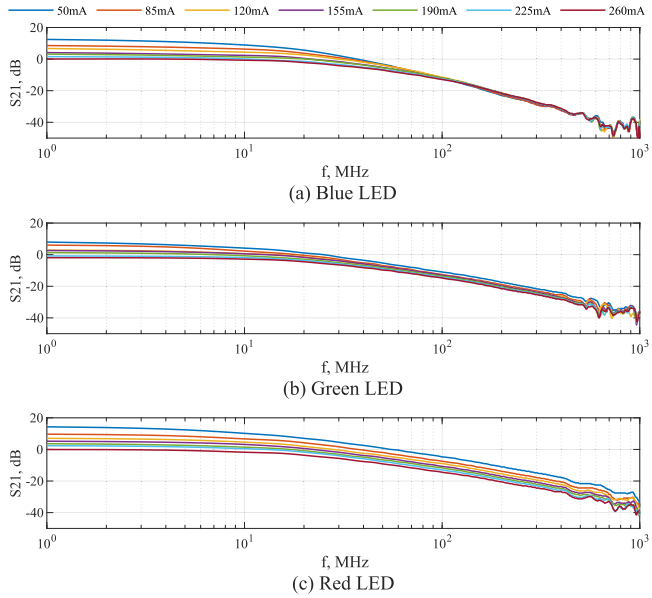

Fig. 6. Responses of the RGB LEDs with different driving currents.

A. System Setup

There are two common methods for achieving white light illumination using LEDs [2]. One approach utilizes blue LEDs combined with wide-band yellow phosphors to generate white light, while the other option employs red, green, and blue (RGB) LEDs. Compared to white LEDs, RGB LEDs offer a broader bandwidth. RGB LEDs exhibit a bandwidth range of 15∼35 MHz, while yellow phosphor-based white LEDs typically reach only a few megahertz. Additionally, RGB LEDs provide the advantage of WDM contributing to an enhanced overall transmission capacity. This enables a VLC system based on tri-color LEDs to achieve a threefold increase in data rate compared to systems using phosphorescent white LEDs. Although, RGB LEDs need independent modulation and biasing, for the sake of broader bandwidth and enhanced system flexibility, RGB LEDs have been employed in this paper. To achieve white light, adjustments in the power ratio for each LED of the same model but with different correlated color temperatures are required [33]. The variations in biasing current, as depicted in Fig. 6, play a crucial role when combining monochromatic lights for illumination purposes.

Then, we designed a driver board based on a bias-T to establish the connection between the LED and the equalizer as shown in Appendix A. Fig. 5 displays the experimental system for visible light communication, where (a) provides an overview of the actual testing environment, while the specific connections are detailed in (b). Tx is the optical signal transmitter that converts electrical signals into optical signals, and GSE refers to the equalizer designed based on the analysis in Section II. An aspheric condenser lens is placed in front of the LED to adjust the divergence angle. The avalanche photodiode module is employed for photoelectric conversion, featuring a flat 3-dB bandwidth exceeding 1 GHz [34], which is sufficient for the testing conducted in this paper. The receiver is also combined with a convex lens for light collection. Usually, filters or/and scatters will also be needed in different application scenarios. The link built in this article only uses convex lenses for collimating and focusing the light to obtain a more extended communication distance. Also, we mainly use short cables and connectors to reduce return loss, as shown in Fig. 5(a). The specific devices involved in Fig. 5 and their models used in the system are listed in Table III. This system also involves two test links as

- To measure S21, S11, etc. with a Vector Network Analyzer (VNA). The VNA's signal output is connected to the signal input of the transmitting board, and the received signal from the receiver is directed into the signal input of the VNA. This enables the measurement of S11 and S21 curves of the link.
- To measure bit error rate (BER), signal-to-noise ratio (SNR), etc. by employing an Arbitrary Waveform Generator (AWG) to generate signals and an Oscilloscope (OSC) to measure parameters like SNR and BER. The AWG is used as a signal source to provide a baseband signal to the transmitting board. Simultaneously, the OSC captures signals from the receiver. The discrete signals collected by the OSC are analyzed to assess the optical path's additional information.

TABLE III
DEVICES USED IN THE SYSTEM

Devices	Name
LED	OSRAM LE RTB N7WM
LENS	THORLABS ACL25416U-A
	THORLABS ACL50832U-A
Photodiode	HAMAMATSU C5658
VNA	RIGOL RSA3015N
AWG	KEYSIGHT M8196A
OSC	RIGOL MSO8104
PA	CREDIT KDT0305A

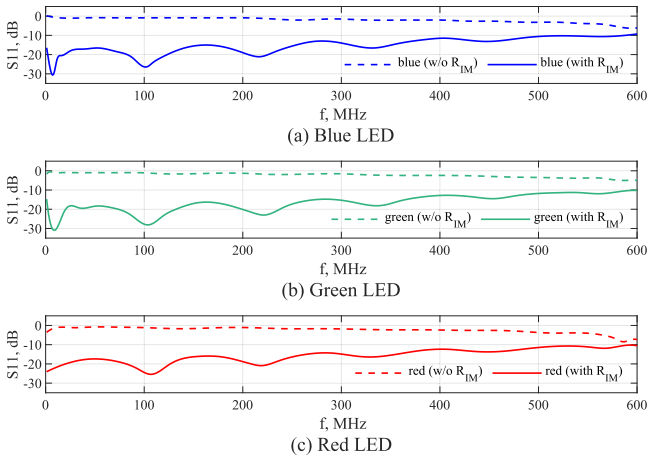

Fig. 7. Comparison of RGB LEDs' S11 curves of drive circuit with and without resistor R_{IM}.

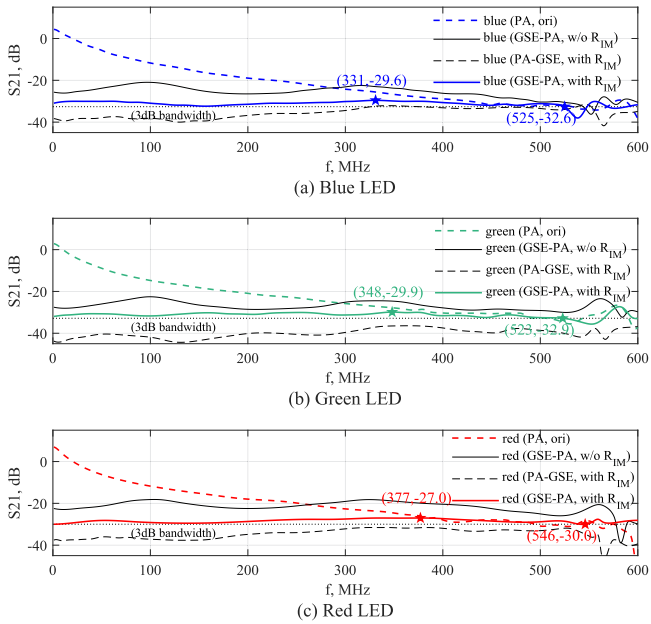

Fig. 8. Test results of the equalizers designed for RGB LEDs. The coloured dashed lines are the original S21 curve.

It is worth noting that the connection arrangement of the Electro-Optical-Electro link remains constant throughout the testing process.

The choice of the operating point is a critical step prior to conducting any tests. According to the equivalent circuit illustrated in Fig. 1 and the (1), it is observed that when the input signal is DC, the gain of the response function is determined by the expression $\frac{r_d}{R_s+R_g}$. However, due to the conducting characteristics of the diode, an increase in the operating current leads to a decrease in the internal resistance r_d, which subsequently results in a reduction in the response amplitude, as depicted in Fig. 6. Contrary to our initial expectations, we observed that a smaller driving current resulted in a higher response amplitude. This unexpected finding challenges the assumption that increasing LED light intensity would enhance the received signal. Additionally, we noted variations in response changes among the three LEDs. As the driving current increases, the low-frequency response of the blue LED experiences significant attenuation, while the high-frequency response remains nearly unchanged. In contrast, both low-frequency and high-frequency responses of the red LED attenuate almost simultaneously. The response changes of the green LED fall between those of the blue LED and red LED. The maximum attenuations of the frequency response for the three RGB LEDs are 12.4 dB, 9.9 dB, and 14.4 dB, respectively, as the driving current varies from 50 mA to 260 mA. Consequently, our selection of an operating point was based on a careful balance between the S21 response, modulation depth, and LED luminous intensity, leading us to decide on a driving current of 150 mA.

B. Bandwidth Evaluation for the Proposed GSE

Based on the first test link described in the previous subsection, this subsection provides the test results for S11 and S21 for the three RGB LEDs, as shown in Figs. 7 and 8. In Fig. 7, the dashed line represents the S11 curve without the impedance-matching resistor R_{IM} (introduced in Appendix A) while the solid line represents the S11 response curve when this resistor is considered. The results show that in the driver circuit without R_{IM} (indicated by the dashed line), a significant portion of the energy is reflected. In contrast, the solid line indicates that a substantial reduction in reflections has been achieved with the inclusion of R_{IM}, indicating successful optimization of the reflection coefficient.

Fig. 8 presents the S21 response curves for the three LEDs before and after equalization. The legend designates GSE for the general second-order equalizer of the transmitter and PA for the power amplifier. Each figure corresponds to the equalization results for a specific LED, with the curves of the blue LED in Fig. 8(a) serving as an illustrative example. The blue dashed line represents the inherent low-pass characteristic of the LED. Subsequently, two configurations involving the equalizer and power amplifier on the emitter board are provided, denoted as GSE-PA and PA-GSE, corresponding to the solid blue line and the black dashed line, respectively. In the GSE-PA configuration, the output signals generated by the AWG first pass through the equalizer before undergoing amplification by the PA. Conversely, in the PA-GSE configuration, the connection order is reversed. Notably, the PA-GSE configuration introduces greater attenuation, since directly connecting the equalizer to the LED leads to suboptimal outcomes, primarily due to the equalization circuit being designed for a 50 Ω load. Consequently, the PA is employed to isolate the equalizer from the LED, mitigating impedance mismatch and ensuring a 50 Ω load for the GSE, all while maintaining low circuit complexity. It is important to mention that, although the PA augments the signal amplitude and, in turn, the SNR of the received signal, extending the bandwidth to approximately 0.5 GHz still necessitates a considerable energy investment.

Furthermore, in Fig. 8(a), we also compared the S21 curves with and without the impedance matching resistor R_{IM},

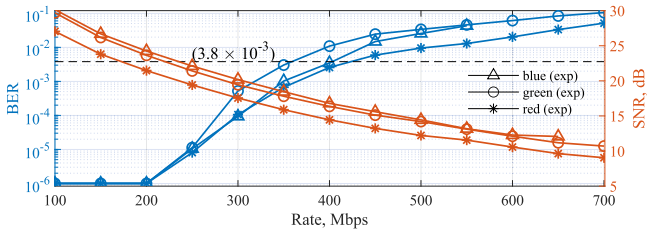

Fig. 9. Measured BER performance with the change of data rate at a distance of 250 cm.

represented by the solid blue and solid black lines under the same connection. The S21 curve without R_{IM} in Fig. 8(a) exhibits significant fluctuations due to intense echoes, while the solid blue line is smoother. It is worth noting that while the direct addition of the resistors R_{IM} is effective, it does consume some energy. Finally, we marked the highest point on the solid blue line in Fig. 8(a), together with the 3-dB bandwidth point by blue stars, and the black dotted line is the reference line for showing the 3-dB bandwidth.

Finally, we extended the bandwidth of the blue LED to 525 MHz from its original 4 MHz. After fine-tuning the parameters of the GSE, we achieved a 3-dB bandwidth of 523 MHz for the green LED and 546 MHz for the red LED, as depicted in Fig. 8(b) and (c), whose initial bandwidths were 7 MHz and 3 MHz, respectively. These bandwidth values shown in Fig. 8, both with and without equalizers, were obtained through measurements as illustrated in Fig. 5. The description of green and red LED parallels blue LED. That is to say, we expanded the 3-dB bandwidth of an RGB LEDs transmitter to more than 1.5 GHz, and this result can fully satisfy IEEE 802.11bb.

C. Data Rate Evaluation of the Proposed GSE

In this subsection, we evaluated the maximum data rate of the proposed transmitter using NRZ-OOK modulation at a distance of 250 cm with a constant signal power. The test results of the maximum data rate are depicted in Fig. 9 with two axes: the left axis represents the increase in BER with rising signal data rates, and the right axis displays the decline in the system's SNR with increasing transmission rates. We measured the power of the signal and noise in the link separately at different data rates [35], and the SNR was calculated as depicted on the right axis of Fig. 9. The theoretical relationship between SNR and data rate can be written as [36]

$$SNR_b = \frac{E_b}{N_0} = \frac{P/R_b}{N_0} = \frac{P}{N_0 R_b}, \tag{7}$$

where E_b represents energy per bit; N_0 is power spectral density of noise; P and R_b are signal power and bit rate respectively. The experimental SNR results in Fig. 9 are consistent with the theoretical analysis, as indicated by (7), where the SNR is inversely proportional to the data rate while the signal power is constant.

The blue, green, and red LEDs can achieve a data rate of 400 Mbps, 350 Mbps, and 400 Mbps respectively within the FEC. The measured NRZ-OOK eye diagrams at 200 Mbps

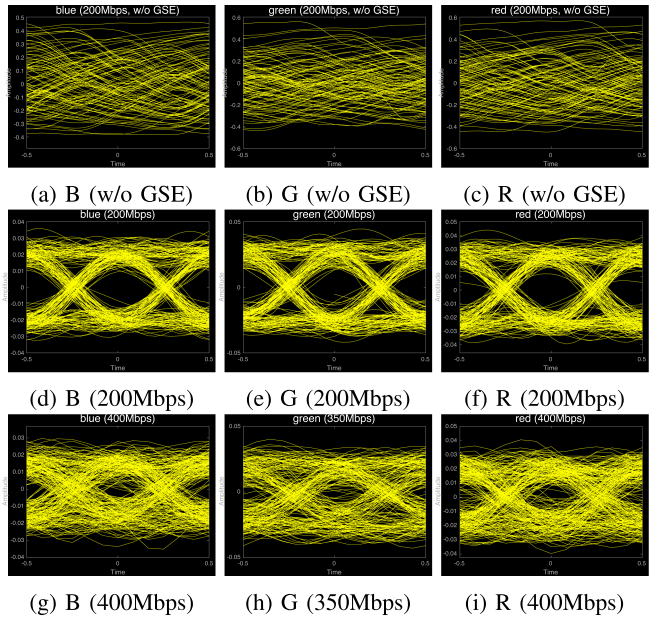

Fig. 10. (a)–(i) Eye diagrams, where (a)–(c) are the eye diagrams without GSE at a rate of 200 Mbps, (d)–(f) are the eye diagrams with the GSE at 200 Mbps, and (g)–(i) are the eye diagrams with the equalizer at higher rates.

are presented in Fig. 10(a)–(c) and (d)–(f) under the configurations of no equalization enabled and GSE enabled. The measurement results show that a completely closed NRZ-OOK eye in Fig. 10(a)–(c) can be opened only with the help of the low-complexity GSE shown in Fig. 4. Fig. 10(g)–(i) depict the eye diagrams at the maximum data rate. It is important to note that the primary focus of this paper is to achieve the ultimate equalization bandwidth using a single commercially available LED with a low-complexity equalizer. For a passive equalizer, it significantly sacrifices signal power for bandwidth expansion. Therefore, when broadening the bandwidth of an LED from several MHz to over 500 MHz, we somewhat overlook the attenuation of signal energy. Balancing the bandwidth and the SNR will be a focal topic of our future work to maximize channel capacity.

To sum up, despite the significant SNR attenuation caused by the equalizer, the designed transmitter can achieve NRZ-OOK data transmission rates of 400 Mbps, 350 Mbps, and 400 Mbps with blue, green, and red LEDs, respectively, at a distance of 250 cm. This means that the designed transmitter can enable communication at a total rate of 1.15 Gbps within the limits of FEC at 3.8×10^{-3}.

IV. Conclusion and Future Work

A general second-order equalizer (GSE) designed for VLC transmitters has been proposed in this paper. This equalizer is developed based on a second-order equivalent circuit model of LEDs utilizing zero-pole matching scheme. Our introduced pre-equalizer, developed from closed-form derivations, effectively extend the bandwidth of individual LEDs to more than 500 MHz, while maintaining lower complexity by utilizing fewer components compared to existing solutions.

To test its real performance, we designed a PCB circuit and verified that the 3-dB bandwidth of GSE in VLC links has been improved largely. Specifically, we showed that the 3-dB bandwidth of a COTS RGB LED-based transmitter can be enlarged from 14 MHz to 1.5 GHz. Our result is consistent with the results in other published literature both in theory and in implementation with lower complexity. Experimental results show that the GSE transmitter can successfully reach a 1.15 Gbps data rate, at a 250 cm distance with a BER below 3.8×10^{-3}. Our results also reveal that the IEEE 802.11bb's 320 MHz LiFi channel bandwidth requirement can be achieved at a very low cost.

The main objective of this work is to develop a low-complexity GSE for ultra-wide bandwidth VLC using cost-effective commercial RGB LEDs, and the receiver SNRs cannot be guaranteed when the bandwidth is larger than 500 MHz. Future efforts may focus on expanding LED's bandwidth, while minimizing the signal distortions at the receiver to approach channel capacity. Specifically, we plan to explore high-order QAM modulations and OFDM as defined in the IEEE 802.11bb standard, to achieve data rate higher than 1.15 Gbps at the same FEC limit. In recognizing the performance limitations of LEDs, researchers could also investigate the use of advanced light sources, such as Super-luminescent Diodes (SLDs) and micro LEDs, for applications requiring both greater bandwidth and larger SNR values. By adopting two GSE links and advanced system designs, we would like to further apply it to a two-way VLC system, such as IEEE 802.11 LiFi links with one access point and one station, to demonstrate its real impact by supporting higher layer communication protocols, like TCP/IP.

APPENDIX A
LED DRIVER

In VLC, a driver circuit serves the dual purpose of supplying the direct current (DC) and implementing alternating current (AC) modulation. [37] categorizes four prevalent modulator types: Linear Mode Modulator, Switching Mode Modulator, Series Switch Modulator, and Parallel Switch Modulator. For this study, we have opted for the Linear Mode Modulator due to its ability to achieve a broader bandwidth and linear waveform modulation. Two common linear modulation methods in VLC are the Bias-T-based and serial-F-based topologies [38]. The serial-F-based topology employs a Field Effect Transistor to couple DC and AC signals while amplifying them simultaneously. In contrast, the Bias-T-based circuit couples signals using a straightforward inductance-capacitor circuit. In our setup, which utilizes common anode RGB LEDs, we have selected the Bias-T-based circuit due to its versatility.

Different from common cathode LEDs or single LEDs, the tri-color LED in our setup is connected to a common anode. Consequently, the signal input is required from the negative electrode. To accommodate this, we have designed the driver circuit, which is depicted in Fig. 11. Fig. 11 illustrates the driver circuit for a single LED within the RGB LEDs. In Fig. 11, we've distinguished the DC loop and AC loop to highlight that the LED is driven by both DC and AC signals simultaneously. Within

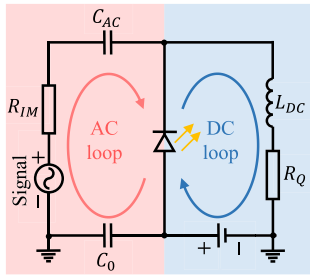

Fig. 11. Driver circuit of a single LED with the DC loop and the AC loop being marked.

the DC loop, a high-inductance inductor L_{DC} is employed to impede the passage of the AC signal, and the quiescent operating point of the LED is adjusted using the series resistance R_Q. In the AC loop, a high capacitance C_{AC} serves to block the passage of the DC biasing current. Capacitor C_0 channels the AC signal to the ground to close the AC loop while simultaneously filtering out DC power noise. The series resistor R_{IM} is designed for impedance matching. Though not the most sophisticated method, it proves effective in practical applications. In essence, the driver circuit comprises a standard Bias-T, resistance R_Q, and resistor R_{IM} meeting the requirements for signal coupling, current control, and impedance matching. A more detailed discussion of the operating point is presented in Section III-B.

APPENDIX B
PROOF OF (5)

We obtain the response function of the equalizer circuit based on Fig. 4(b), which can be denoted as

$$
\begin{aligned}
H_{\mathrm{E}}(s) &= \frac{(sL+R_1)//\left(\frac{1}{sC}//R_2+R_L\right)}{R_g+(sL+R_1)//\left(\frac{1}{sC}//R_2+R_L\right)} \frac{R_L}{\frac{1}{sC}//R_2+R_L} \\
&\overset{(a)}{=} \frac{R_L\left(sL+R_1\right)\left(sCR_2+1\right)}{\begin{bmatrix} s^2\,LCR_2\left(R_g+R_L\right)+s[L\left(R_2+R_g+R_L\right) \\ +CR_2\left(R_1R_g+R_1R_L+R_gR_L\right)] \\ +R_1R_2+R_1\left(R_g+R_L\right)+R_gR_L+R_2R_g \end{bmatrix}} \\
&= \frac{R_L\left(sL+R_1\right)\left(sCR_2+1\right)}{\begin{bmatrix} \left(sL+R_1+\frac{R_gR_L}{R_g+R_L}\right)[sCR_2\left(R_g+R_L\right) \\ +R_2+R_g+R_L] \end{bmatrix}+R_2\left(R_g-\frac{R_gR_L}{R_g+R_L}\right)} \\
&\overset{(b)}{=} \frac{R_g\left(sL+R_1\right)\left(sCR_2+1\right)}{\left(sL+R_1+\frac{1}{2}R_g\right)\left(2\,sCR_2R_g+R_2+2R_g\right)+\frac{1}{2}R_2R_g} \\
&= \frac{\frac{2R_gR_1}{(2R_1+R_g)(2R_g+R_2)}\left[\frac{s}{\frac{R_1}{L}}+1\right]\left[\frac{s}{\frac{1}{CR_2}}+1\right]}{\left[\frac{s}{\frac{2R_1+R_g}{2L}}+1\right]\left[\frac{s}{\frac{2R_g+R_2}{2CR_gR_2}}+1\right]+\frac{R_gR_2}{(2R_1+R_g)(2R_g+R_2)}} \\
&\overset{(c)}{\approx} \frac{\frac{2R_gR_1}{(2R_1+R_g)(2R_g+R_2)}\left(\frac{s}{\omega_{\mathrm{E1,I}}}+1\right)\left(\frac{s}{\omega_{\mathrm{E2,I}}}+1\right)}{\left(\frac{s}{\omega_{\mathrm{E3,I}}}+1\right)\left(\frac{s}{\omega_{\mathrm{E4,I}}}+1\right)},
\end{aligned}
\tag{8}
$$

where

- (a) follows from $a\,//\,b \triangleq \frac{ab}{a+b}$;

- (b) follows from $R_L = R_g = 50\Omega$;
- (c) follows because the precise poles in (b) within the denominator can only be determined by the roots of the quadratic equation. This approach would yield complex and intricate expressions, potentially obscuring the underlying relationships. In contrast, we selected an alternative factorization in (c) to attain a more succinct and intuitive expression. Note that the approximation in (c) is not a numerical approximation. Since its impact is confined to the reference expression associated with the 3 dB bandwidth. Importantly, it doesn't affect the outcomes of the zero-pole matching process. Therefore, for the sake of clarity and conciseness, we boldly made this approximation to facilitate a more intuitive presentation.

This proves (5).

REFERENCES

[1] E. C. Strinati et al., "6G: The next frontier: From holographic messaging to artificial intelligence using subterahertz and visible light communication," *IEEE Veh. Technol. Mag.*, vol. 14, no. 3, pp. 42–50, Sep. 2019.

[2] M. T. Rahman, A. S. M. Bakibillah, R. Parthiban, and M. Bakaul, "Review of advanced techniques for multi-gigabit visible light communication," *IET Optoelectron.*, vol. 14, no. 6, pp. 359–373, 2020.

[3] *IEEE Standard for Local and Metropolitan Area Networks–Part 15.7: Short-Range Optical Wireless Communications*, IEEE Standard 802.15.7-2011, Sep. 6, 2019.

[4] *VLC high speed indoor visible light communication transceiver–system architecture, physical layer and data link layer specification*, Rec. G.9991, ITU, Geneva, Switzerland, 2019.

[5] "Status of IEEE 802.11 light communication TG," 2018. [Online]. Available: http://www.ieee802.org/11/Reports/tgbb_update.htm

[6] "Wireless LAN Medium Access Control (MAC) and Physical Layer (PHY) Specifications Amendment 7: Light Communications," 2023. [Online]. Available: https://standards.ieee.org/ieee/802.11bb/10823/

[7] A. A. Purwita and H. Haas, "IQ-WDM for IEEE 802.11 bb-based LiFi," in *Proc. IEEE Wireless Commun. Netw. Conf.*, 2020, pp. 1–6.

[8] J. Grubor, S. C. J. Lee, K.-D. Langer, T. Koonen, and J. W. Walewski, "Wireless high-speed data transmission with phosphorescent white-light LEDs," in *Proc. IEEE 33rd Eur. Conf. Exhib. Opt. Commun.-Post-Deadline Papers*, 2007, pp. 1–2.

[9] H. Le Minh et al., "High-speed visible light communications using multiple-resonant equalization," *IEEE Photon. Technol. Lett.*, vol. 20, no. 14, pp. 1243–1245, Jul. 2008.

[10] H. Le Minh et al., "80 Mbit/s visible light communications using pre-equalized white LED," in *Proc. IEEE 34th Eur. Conf. Opt. Commun.*, 2008, pp. 1–2.

[11] X. Huang, J. Shi, J. Li, Y. Wang, Y. Wang, and N. Chi, "750Mbit/s visible light communications employing 64QAM-OFDM based on amplitude equalization circuit," in *Proc. IEEE Opt. Fiber Commun. Conf. Exhib.*, 2015, pp. 1–3.

[12] Y. Wang, X. Huang, L. Tao, J. Shi, and N. Chi, "4.5-Gb/s RGB-LED based WDM visible light communication system employing CAP modulation and RLS based adaptive equalization," *Opt. Exp.*, vol. 23, no. 10, pp. 13626–13633, 2015.

[13] Z. Zhang et al., "Over 700 MHz-3 dB bandwidth UOWC system based on blue HV-LED with T-bridge pre-equalizer," *IEEE Photon. J.*, vol. 11, no. 3, Jun. 2019, Art. no. 7903812.

[14] C. Min et al., "A novel method for constructing VLC equalizer with active-passive hybrid network," *IEEE Photon. J.*, vol. 12, no. 2, Apr. 2020, Art. no. 7500310.

[15] L. Tang, Y. Wu, Z. Cheng, D. Teng, and L. Liu, "Over 23.43 Gbps visible light communication system based on 9 V integrated RGBP LED modules," *Opt. Commun.*, vol. 534, 2023, Art. no. 129317.

[16] L. Zeng, D. O'Brien, H. Le-Minh, K. Lee, D. Jung, and Y. Oh, "Improvement of date rate by using equalization in an indoor visible light communication system," in *Proc. IEEE 4th Int. Conf. Circuits Syst. Commun.*, 2008, pp. 678–682.

[17] H. Li, X. Chen, B. Huang, D. Tang, and H. Chen, "High bandwidth visible light communications based on a post-equalization circuit," *IEEE Photon. Technol. Lett.*, vol. 26, no. 2, pp. 119–122, Jan. 2014.

[18] X. Li, B. Hussain, L. Wang, J. Jiang, and C. P. Yue, "Design of a 2.2-mW 24-Mb/s CMOS VLC receiver SoC with ambient light rejection and post-equalization for Li-Fi applications," *J. Lightw. Technol.*, vol. 36, no. 12, pp. 2366–2375, Jun. 2018.

[19] Q. Lu, J. Chen, Y. Zhao, and N. Chi, "Super Gaussian kernel-aided deep neural network equalizer utilized in visible light transparent transmission from free-space to fiber," in *Proc. IEEE Int. Conf. Wireless Commun. Signal Process.*, 2020, pp. 353–357.

[20] P. Miao, W. Yin, H. Peng, and Y. Yao, "Study of the performance of deep learning-based channel equalization for indoor visible light communication systems," *Photonics*, vol. 8, 2021, Art. no. 453.

[21] S. Li, Y. Zou, Z. Shi, J. Tian, and W. Li, "Performance enhancement of CAP-VLC system utilizing GRU neural network based equalizer," *Opt. Commun.*, vol. 528, 2023, Art. no. 129062.

[22] C. Chen et al., "Digital pre-equalization for OFDM-based VLC systems: Centralized or distributed?," *IEEE Photon. Technol. Lett.*, vol. 33, no. 19, pp. 1081–1084, Oct. 2021.

[23] W. Xu, M. Zhang, D. Han, Z. Ghassemlooy, P. Luo, and Y. Zhang, "Real-time 262-Mb/s visible light communication with digital predistortion waveform shaping," *IEEE Photon. J.*, vol. 10, no. 3, Jun. 2018, Art. no. 7903610.

[24] X. Li, Z. Ghassemlooy, S. Zvanovec, R. Perez-Jimenez, and P. A. Haigh, "Should analogue pre-equalisers be avoided in VLC systems?" *IEEE Photon. J.*, vol. 12, no. 2, Apr. 2020, Art. no. 7901014.

[25] R. Kisacik, M. Y. Yagan, M. Uysal, A. E. Pusane, and A. D. Yalcinkaya, "A new LED response model and its application to pre-equalization in VLC systems," *IEEE Photon. Technol. Lett.*, vol. 33, no. 17, pp. 955–958, Sep. 2021.

[26] L. Wang, X. Wang, J. Kang, and C. P. Yue, "A 75-Mb/s RGB PAM-4 visible light communication transceiver system with pre-and post-equalization," *J. Lightw. Technol.*, vol. 39, no. 5, pp. 1381–1390, Mar. 2020.

[27] R. Kısacık et al., "A 130 nm CMOS receiver for visible light communication," *J. Lightw. Technol.*, vol. 40, no. 12, pp. 3681–3687, Jun. 2022.

[28] P. Salvador, J. Valls, J. L. Corral, V. Almenar, and M. J. Canet, "Linear response modeling of high luminous flux phosphor-coated white LEDs for VLC," *J. Lightw. Technol.*, vol. 40, no. 12, pp. 3761–3767, Jun. 2022.

[29] X. Li, Z. Ghassemlooy, S. Zvanovec, M. Zhang, and A. Burton, "Equivalent circuit model of high power LEDs for VLC systems," in *Proc. IEEE 2nd West Asian Colloq. Opt. Wireless Commun.*, 2019, pp. 90–95.

[30] X. Li, Z. Ghassemlooy, S. Zvanovec, and L. N. Alves, "An equivalent circuit model of a commercial LED with an ESD protection component for VLC," *IEEE Photon. Technol. Lett.*, vol. 33, no. 15, pp. 777–779, Aug. 2021.

[31] J. M. Senior and M. Y. Jamro, *Optical Fiber Communications: Principles and Practice*. London, U.K.: Pearson Educ., 2009.

[32] R. Zhang, J. Xiong, M. Li, and L. Lu, "Implementation of a low-complexity pre-equalizer for visible light communications," in *Proc. 9th Int. Conf. Comput. Commun.*, 2023.

[33] J. Xiong, R. Zhang, L. Lu, Q. T. Sun, and K. Long, "Physical-layer network coding enhanced visible light communications using RGB LEDs," *IEEE Photon. J.*, vol. 15, no. 1, Feb. 2023, Art no. 7301010.

[34] "APD module, C5658," 2019. [Online]. Available: https://www.hamamatsu.com/content/dam/hamamatsu-photonics/sites/documents/99_SALES_LIBRARY/ssd/c5658_kacc1023e.pdf

[35] J. G. Proakis, *Digital Signal Processing: Principles, Algorithms, and Applications*. Bengaluru, India: Pearson Educ. India, 2007.

[36] J. G. Proakis, *Digital Communications*. New York, NY, USA: McGraw-Hill, 2008.

[37] L. Teixeira, F. Loose, J. M. Alonso, C. H. Barriquello, V. A. Reguera, and M. A. Dalla Costa, "A review of visible light communication LED drivers," *IEEE Trans. Emerg. Sel. Topics Power Electron.*, vol. 10, no. 1, pp. 919–933, Feb. 2022.

[38] X. Deng, K. Arulandu, Y. Wu, S. Mardanikorani, G. Zhou, and J.-P. M. G. Linnartz, "Modeling and analysis of transmitter performance in visible light communications," *IEEE Trans. Veh. Technol.*, vol. 68, no. 3, pp. 2316–2331, Mar. 2019.